How to cite: *Angew. Chem. Int. Ed.* **2023**, *62*, e202307884
doi.org/10.1002/anie.202307884

On-Surface Synthesis Hot Paper

On-Surface Synthesis and Characterization of a High-Spin Aza-[5]-Triangulene

Manuel Vilas-Varela[+], Francisco Romero-Lara[+], Alessio Vegliante, Jan Patrick Calupitan, Adrián Martínez, Lorenz Meyer, Unai Uriarte-Amiano, Niklas Friedrich, Dongfei Wang, Fabian Schulz, Natalia E. Koval, María E. Sandoval-Salinas, David Casanova, Martina Corso, Emilio Artacho, Diego Peña, and José Ignacio Pascual**

Abstract: Triangulenes are a class of open-shell triangular graphene flakes with total spin increasing with their size. In the last years, on-surface-synthesis strategies have permitted fabricating and engineering triangulenes of various sizes and structures with atomic precision. However, direct proof of the increasing total spin with their size remains elusive. In this work, we report the combined in-solution and on-surface synthesis of a large nitrogen-doped triangulene (aza-[5]-triangulene) on a Au(111) surface, and the detection of its high-spin ground state. Bond-resolved scanning tunneling microscopy images uncovered radical states distributed along the zigzag edges, which were detected as weak zero-bias resonances in scanning tunneling spectra. These spectral features reveal the partial Kondo screening of a high-spin state. Through a combination of several simulation tools, we find that the observed distribution of radical states is explained by a quintet ground state ($S=2$), instead of the quartet state ($S=3/2$) expected for the neutral species. This confirms that electron transfer to the metal substrate raises the spin of the ground state. We further provide a qualitative description of the change of (anti)aromaticity introduced by N-substitution, and its role in the charge stabilization on a surface, resulting in an $S=2$ aza-triangulene on Au(111).

Triangulenes are triangular-shaped polybenzenoid hydrocarbons with edges formed by n zig-zag units (hence, [n]-triangulene) and non-zero electronic spin ground state. The π-conjugated lattice of [n]-triangulene is frustrated, depicting a non-Kekulé structure with n-1 unpaired π-electrons,[1–5] forming an electronic ground state with a net spin $S=(n-1)/2$.[6] The linear increase of spin state with the triangulene size n endows these systems with a strong potential for becoming functional platforms for molecular spintronics and quantum computing applications.[1,7–10]

Owing to their open-shell character, the solution synthesis of triangulenes is very challenging.[11–13] Lately, on-surface-synthesis (OSS) strategies[14,15] have demonstrated to be a viable route for the fabrication of atomically perfect triangulenes with increasing size[16–20] (some of these shown in Figure 1a). Interestingly, OSS can also produce more complex triangulene nanostructures,[21–27] with a variety of magnetic properties emerging from the exchange interaction between triangulene units. Overall, the net spin state of triangulene derivatives is associated with an imbalance in

[*] Dr. M. Vilas-Varela,[+] A. Martínez, Prof. Dr. D. Peña
Centro Singular de Investigación en Química Biolóxica e Materiais Moleculares (CiQUS) and Departamento de Química Orgánica, Universidade de Santiago de Compostela
15782-Santiago de Compostela (Spain)
E-mail: diego.pena@usc.es

F. Romero-Lara,[+] A. Vegliante, L. Meyer, U. Uriarte-Amiano, Dr. N. Friedrich, Dr. D. Wang, Dr. F. Schulz, Dr. N. E. Koval, Prof. E. Artacho, Prof. J. I. Pascual
CIC nanoGUNE-BRTA
20018 Donostia-San Sebastián (Spain)
E-mail: ji.pascual@nanogune.eu

Dr. J. P. Calupitan0000-0003-3044-2603, Dr. M. Corso
Centro de Física de Materiales CSIC/UPV-EHU-Materials Physics Center
20018 Donostia-San Sebastián (Spain)
Homepage: 0000-0003-3044-2603

Dr. J. P. Calupitan0000-0003-3044-2603, Dr. D. Casanova
Donostia International Physics Center (DIPC)
20018 Donostia-San Sebastián (Spain)

Dr. M. E. Sandoval-Salinas
School of Physical and Chemical Sciences, Queen Mary University of London (UK)

Dr. D. Casanova, Prof. E. Artacho, Prof. J. I. Pascual
Ikerbasque, Basque Foundation for Science
48009 Bilbao (Spain)

Prof. E. Artacho
Theory of Condensed Matter, Cavendish Laboratory, University of Cambridge
J. J. Thomson Ave., Cambridge CB3 0HE (UK)

[+] These authors contributed equally to this work.

© 2023 The Authors. Angewandte Chemie International Edition published by Wiley-VCH GmbH. This is an open access article under the terms of the Creative Commons Attribution Non-Commercial NoDerivs License, which permits use and distribution in any medium, provided the original work is properly cited, the use is non-commercial and no modifications or adaptations are made.

 © 2023 The Authors. Angewandte Chemie International Edition published by Wiley-VCH GmbH

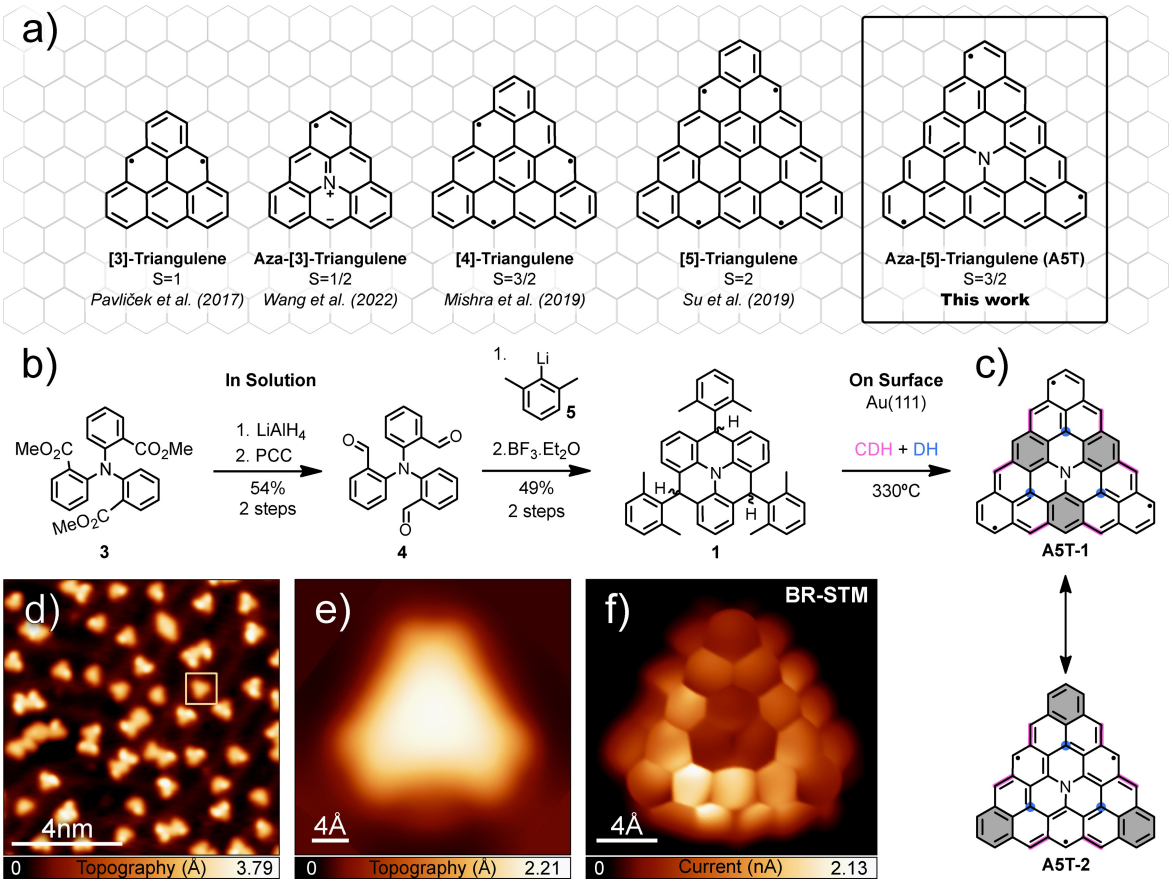

Figure 1. **a)** Selected previously studied triangulene nanostructures of different sizes and doping. **b)** Synthetic route to obtain the A5T precursor **1** by solution chemistry. **c)** Two resonance structures of target A5T showing different locations of Clar sextets (in grey) and π-radicals. The C–C bonds highlighted in purple indicate the ones formed via on-surface assisted cyclodehydrogenation (CDH). The blue spots mark the sites where H atoms were removed via on-surface assisted dehydrogenation (DH). **d)** Resulting STM image ($V=1.5$ V, $I=10$ pA) of molecular precursor **1** deposited on a Au(111) surface after annealing the sample to 330 °C. Yellow square indicates a fully planar structure. **e)** STM image ($V=1$ V, $I=10$ pA) of the A5T. **f)** Constant-height bond-resolved STM (BR-STM) image ($V=5$ mV) of the A5T performed with a CO-functionalized tip. Experimental data was analyzed using WsXM.[57]

the number of carbon sites in the two alternating triangular sub-lattices (N_A and N_B), following Ovchinnikov's rule[6] $S=1/2\ |N_A–N_B|$.

In addition to tailoring the nanographene's shape and size, OSS strategies have also been applied to insert heteroatoms or functional groups for modifying the electronic properties of graphene-based nanostructures.[28–35] Ovchinnikov[6] predicted that heteroatom substitution in alternant sublattices acts as a defect that modifies the sublattice imbalance and, hence, the resulting spin state.[36,37] However, recent results on aza-[3]-triangulene (A3T)[12,35,38] found that the nitrogen substitution in minority sites reduces the spin state from $S=1$ in all-carbon [3]-triangulene (3T) to $S=1/2$ in A3T. This apparently contradicts Ovchinnikov's prediction that a larger spin ground state ($S=3/2$ in A3T) shall be expected when minority sites are removed. Investigation of this apparent paradox requires experimental access to larger triangulene structures and determination of their spin state.

Despite the successful imaging of triangulenes on metal surfaces using low-temperature scanning tunneling microscopy (STM),[17–20,35,39] the resolution of their intrinsic spin state has been hampered by the lack of spin-sensitive signals. Owing to the very weak magnetic anisotropy of carbon systems, the π-magnetism is isotropic and paramagnetic, thus difficult to access by spin-polarized scanning tunneling microscopy.[40] Instead, a zero-bias resonance due to the Kondo-screening[41,42] of spins by the metallic substrate has been normally used as an unequivocal fingerprint of a spin-polarized ground state in triangulenes.[20,35,43] Unfortunately, the universal behavior of Kondo screening determines that the associated zero-bias resonance decreases its intensity with increasing spin values,[22,35,44] requiring very low temperatures for its detection.

In this work, we present an OSS strategy for engineering a large nitrogen-doped triangulene, the aza-[5]-triangulene (A5T, rectangle in Figure 1a), and demonstrate that it lies in an $S=2$ ground state on a Au(111) surface. The synthesis route involved the targeted thermal cyclodehydrogenation of a tri-substituted A3T derivative (**1** in Figure 1b) over the gold substrate. Combining bond-resolved STM and spectral maps of the density of states close to the Fermi level, we

© 2023 The Authors. Angewandte Chemie International Edition published by Wiley-VCH GmbH

15213773, 2023, 41, Downloaded from https://onlinelibrary.wiley.com/doi/10.1002/anie.202307884 by Universidade de Santiago de Compostela, Wiley Online Library on [31/10/2023]. See the Terms and Conditions (https://onlinelibrary.wiley.com/terms-and-conditions) on Wiley Online Library for rules of use; OA articles are governed by the applicable Creative Commons License

show that A5T lies in a high-spin ground state, comprised of four singly occupied states. Our density functional theory (DFT) simulations reveal that the nitrogen heteroatom, located in the majority sublattice in A5T, reduces the $S=2$ spin of the pristine [5]-triangulene (5T) down to 3/2. Although this coincides with the prediction by Ovchinnikov's rule, the origin is caused by the addition of an extra electron in the π-conjugated system, donated by the N atom, which also induces a marked anti-aromatic character around the aza group. On the metal substrate, the A5T system transfers this extra electron to the metal underneath, i.e., it is oxidized to $A5T^+$, recovering the quintet ground state of the parent 5T flake. These results validate predictions for high-spin nanographenes[18,45] and further demonstrate that such a high-spin state survives over a metallic substrate.

Inspired by the precursor design used by Su et al. for the generation of 5T,[18] we envisioned the synthesis of A5T by on-surface planarization of the A3T derivative **1**, which is substituted with three dimethylphenyl groups (Figure 1b). Compound **1** was obtained by solution chemistry in four steps from amine **3**.[35] First, sequential treatment with lithium aluminum hydride ($LiAlH_4$), followed by oxidation with pyridinium chlorochromate (PCC) afforded trialdehyde **4** in 54 % yield. Then, the addition of three equivalents of organolithium derivative **5**, followed by BF_3-promoted three-fold intramolecular Friedel–Crafts, led to the formation of the A5T precursor **1** in 49 % yield.

Precursor **1** was deposited on an Au(111) substrate at room temperature and in ultra-high vacuum conditions. To obtain the targeted A5T, six new C–C bonds had to be created, and twenty one hydrogen atoms had to be removed from its bulky three-dimensional structure. We annealed the pre-covered substrate to 330 °C (see methods) to induce cyclodehydrogenation (CDH) and dehydrogenation (DH) of the precursor and obtained a sample with planar molecular platforms, as we confirmed using low-temperature STM. Images like in Figure 1d resolve that some molecules appeared with some bright lobes corresponding to sp^3 carbon atoms surviving the CDH/DH step, while others underwent covalent couplings between flakes forming larger structures (supplementary Figure S1). Nevertheless, about 10 % of the monomers appear fully planarized. Some of them appear with a few extra hydrogen atoms, which can be controllably removed by bias pulses (Figure S2, S3 and S4); others correspond to the targeted A5T molecule (square in Figure 1d, zoomed in Figure 1e).

Figure 1f shows a high-resolution STM image of the intact A5T flake from Figure 1e, obtained with a CO-functionalized tip at a low bias (typically ≤ 5 mV) and scanning in constant-height mode with low tunneling resistances.[49,50] This allows us to achieve a bond-resolved (BR) image that shows the honeycomb lattice of the A5T and confirms the successful synthesis. In some cases, remnant H atoms from incomplete CDH show up in the BR images as deformations of the zigzag edges (e.g., as in Figure S3 and S4). However, they were removed by high-energy electron tunneling,[43] until the final product, A5T, was obtained, like in Figure 1f. Interestingly, the current contrast in the BR images is not homogeneous across the A5T backbone but appears higher along zigzag edges (with small variations of intensity between rings probably caused by non-planar adsorption due to the Au(111) herringbone reconstruction) and darker at the center and at the three vertices. The larger current over the edges suggests the presence of zero-energy features, normally related to spin states. The lower tunneling current over the A5T center is probably due to both the absence of zero-energy features and a small out-of-plane distortion of the N towards the Au(111) surface. The darker rings at the vertices also claim spin-free regions, such as one would expect if highly stable Clar sextets[51,52] were localized at these sites. Tentatively, we compare this tunneling current distribution with the dominant resonant structures expected for A5T (Figure 1c) and find that structure **A5T-2** appears closer to the experimental tunneling current maps.

In order to experimentally address the spin ground state of A5T, we performed tunneling spectroscopy at $T=1.2$ K, measuring the low-bias differential conductance signal (dI/dV) over various parts of the molecule. Figure 2a shows dI/dV spectra taken at the zigzag edges of the A5T molecule (colored dots in Figure 2b). Narrow zero-bias spectral peaks reveal the existence of a Kondo-screened spin state at these sites. To capture the spatial distribution of the spin signal, we measured a spectral profile along the edges of the A5T molecule (Figure 2c). The Kondo resonance extends along the zigzag edges with its maximum intensity above the central ring but decreases towards the vertices, as well as over the central region of the molecule as in Figure S5. This distribution of the Kondo signal agrees with the tunneling current variations of the BR images (bright zigzag edges and dark vertices). The map of Figure 2c also reveals that the amplitude of the Kondo peak is very small, only slightly larger than the small inelastic steps at ± 5 mV (also in Figure S5) attributed to the excitation of the frustrated translational vibrational mode of the CO molecule attached to the tip apex.[53]

The narrow linewidth (FWHM <2 mV) of the Kondo resonances is consistent with a Kondo temperature ~ 10 K (Figure 2a), larger than the temperature of the measurement, indicating that the A5T molecules lie in the strong-coupling Kondo regime. However, zero-bias peaks with such a small amplitude are normally observed when the molecular system has a spin larger than $S=1/2$, and the Kondo effect at the measuring temperature only applies to some of the spin channels, i.e., an underscreened Kondo effect.[22] The underscreened Kondo character of A5T can be further demonstrated by measuring the evolution of the zero-bias resonance under increasing magnetic fields. Figure 2d shows the spectra measured on the green spot marked in Figure 2b as the magnetic field is ramped up to 2.9 T. The Kondo resonance splits already for low values of the magnetic field, instead of slowly broadening with increasing magnetic field, as expected for a fully screened case.[43] As shown in the inset of Figure 2d, the splitting energy follows the Zeeman energy of an $S=1/2$ in a magnetic field, indicating that the Kondo screening is not complete.[22] Hence, the Kondo feature suggests a large spin ground state for A5T, but we cannot obtain a precise indication of its total spin from its

© 2023 The Authors. Angewandte Chemie International Edition published by Wiley-VCH GmbH

15213773, 2023, 41, Downloaded from https://onlinelibrary.wiley.com/doi/10.1002/anie.202307884 by Universidade de Santiago de Compostela, Wiley Online Library on [31/10/2023]. See the Terms and Conditions (https://onlinelibrary.wiley.com/terms-and-conditions) on Wiley Online Library for rules of use; OA articles are governed by the applicable Creative Commons License

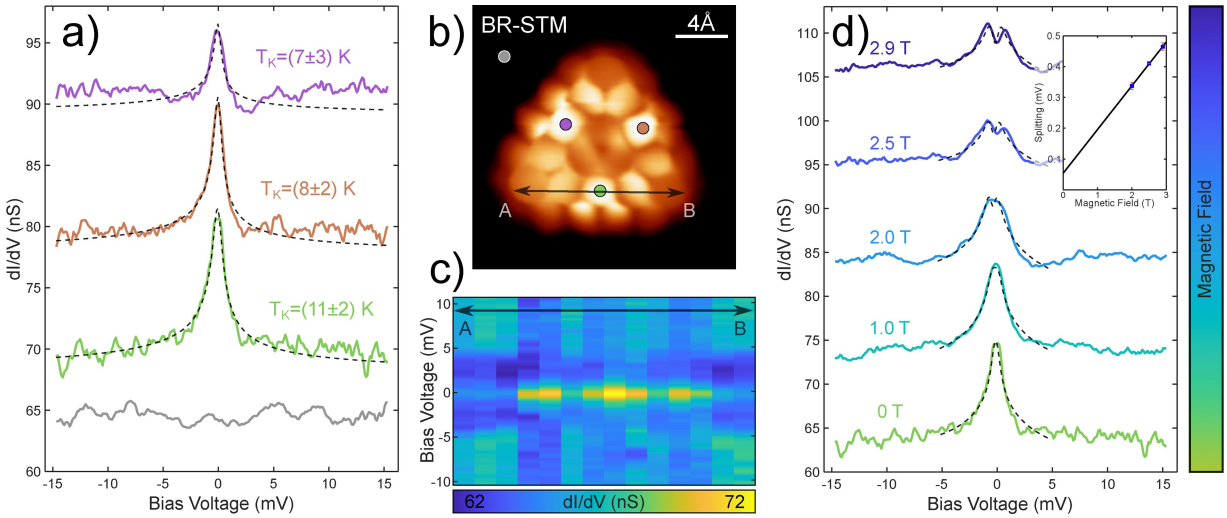

Figure 2. **a)** Low-energy *dI/dV* spectra taken on the spots marked by colored circles in b) at $T=1.2$ K. Dashed lines are fits of the three spectra using a Frota function,[46] from which the indicated Kondo temperatures ($T_K=(\mathrm{FWHM}^2-(2\pi k_B T)^2)^{1/2}/2k_B$[47]) are estimated assuming a strong-coupling Kondo regime ($T<T_K$). Spectra are vertically shifted for clarity. **b)** BR-STM image ($V=5$ mV) of A5T. **c)** Low-energy *dI/dV* spectral line along one edge of A5T, marked by an arrow in b), obtained with a CO-functionalized tip. **d)** Magnetic field-dependent low-energy *dI/dV* measurements. Spectra were taken on the green spot marked in b). Dashed lines correspond to the fits of the Kondo resonances in a magnetic field for a spin-2 model including third-order terms with the code from Ternes.[48] Spectra are shifted vertically for clarity. The inset shows the average splitting of the Kondo peak fits as a function of the magnetic field for three sets of measurements (on each of the spots of the A5T in image b)). The splitting follows the line $E_{ZS}=g\cdot\mu_B\cdot S\cdot B$ with a fitted $g=1.23\pm0.12$. More details about the procedure are in Figure S4.

magnetic field dependence. This is because, in the absence of magnetic anisotropy, the splitting of the Kondo resonance always follows $g\cdot\mu_b$, the $S=1/2$ Zeeman excitation energy.[44]

To find out the spin state, we study the frontier orbitals using *dI/dV* maps and compare them to results from DFT and mean-field Hubbard (MFH) simulations (see methods). Figure 3a shows a set of selected differential conductance maps at different bias values around zero bias, i.e. Fermi level (see Figure S7 for additional bias values in the range of −1.85 to 2.05 V). Albeit *dI/dV* spectra do not show marked resonances, the *dI/dV* maps exhibit clear shapes, corresponding to the local density of states of the different molecular orbitals of A5T. Figure 3b and 3c show the wavefunctions and the energy level diagram, respectively, of the spin-unrestricted orbitals of A5T computed by DFT (see methods) around the Fermi level (±0.75 eV). The C_{3v} symmetry of the molecule on the surface imposes degeneracy into ψ_1 and ψ_2 orbitals while the two others remain non-degenerate. For the case of A5T (mid-panel in Figure 3c), $\psi_1^{o(u)}$, $\psi_2^{o(u)}$, and $\psi_3^{o(u)}$ correspond to the singly (un)occupied molecular orbitals SOMO (SUMO), while ψ_4 remains fully occupied. This results in an $S=3/2$ spin ground state, also in good agreement with MFH calculations in Figure S8.

To reveal the spin state on the surface, we compare the orbital distribution of the computed SOMOs with the *dI/dV* maps of Figure 3a. The most important feature here is that the zero-bias map, which reproduces the amplitude distribution of the Kondo resonance, follows the characteristic shape of the ψ_4 orbital, accounting for a larger signal on the edges than on the vertices. This indicates that ψ_4 is the Kondo-screened state, evidencing its singly occupied character on the Au(111) substrate, as it would be in the case of the cationic species A5T$^+$ in the right panel of Figure 3c. The rest of the SOMOs can be also recognized in the *dI/dV* maps of Figure 3a ($\psi^{o}_{1,2}$ at ~−1.15 eV, and the correlated pair ψ^{o}_3 and ψ^{u}_3 at ~−0.15 eV and 0.25 eV, respectively). In other words, the $S=2$ ground state is a consequence of the charge donation from $\psi_4^{o/u}$ to the surface resulting in a positively charged molecule, as similarly observed in A3T.[1]

The effect of the N heteroatom substitution can be deduced by comparing its orbital structure with that of the all-carbon [5]-triangulene (5T).[18] Owing to its particular topology, 5T has four SOMOs, i.e., a nullity $\eta=4$.[1] This gives rise to an $S=2$ ground state in the presence of Coulomb correlations, as confirmed by DFT (Figure 3c and Figure S9) and MFH (Figure S8). Substituting the central carbon atom with a nitrogen atom does not distort the orbital shapes (see orbital shapes of 5T in Figure S8 and S9), but simply adds an extra electron into the π-conjugated network. This "extra" π-electron populates the ψ_4 state, which is the state with the largest amplitude at the N site (Figure 3b and Figure S7), and consequently reduces the spin to $S=3/2$ (from left to mid panel in Figure 3c). Contrary to the smaller A3T, the extra electron does not lead to Jahn–Teller distortions,[38] because here it populates a non-degenerate level. Consequently, the lack of stabilizing Jahn–Teller distortion keeps the ψ_4 state closer to the Fermi level than the other frontier orbitals. Therefore, the electron added by the N heteroatom to the conjugated π-system remains the most valent and is donated to the Au(111) substrate, eventually leading to the oxidized A5T (A5T$^+$), which adopts the $S=2$ ground state of 5T on the surface.

Spectral maps of Kondo-amplitude like in Figure 1f, 2b and 3a resolved a peculiar pattern of unpaired electron

© 2023 The Authors. Angewandte Chemie International Edition published by Wiley-VCH GmbH

15213773, 2023, 41, Downloaded from https://onlinelibrary.wiley.com/doi/10.1002/anie.202307884 by Universidade de Santiago de Compostela, Wiley Online Library on [31/10/2023]. See the Terms and Conditions (https://onlinelibrary.wiley.com/terms-and-conditions) on Wiley Online Library for rules of use; OA articles are governed by the applicable Creative Commons License

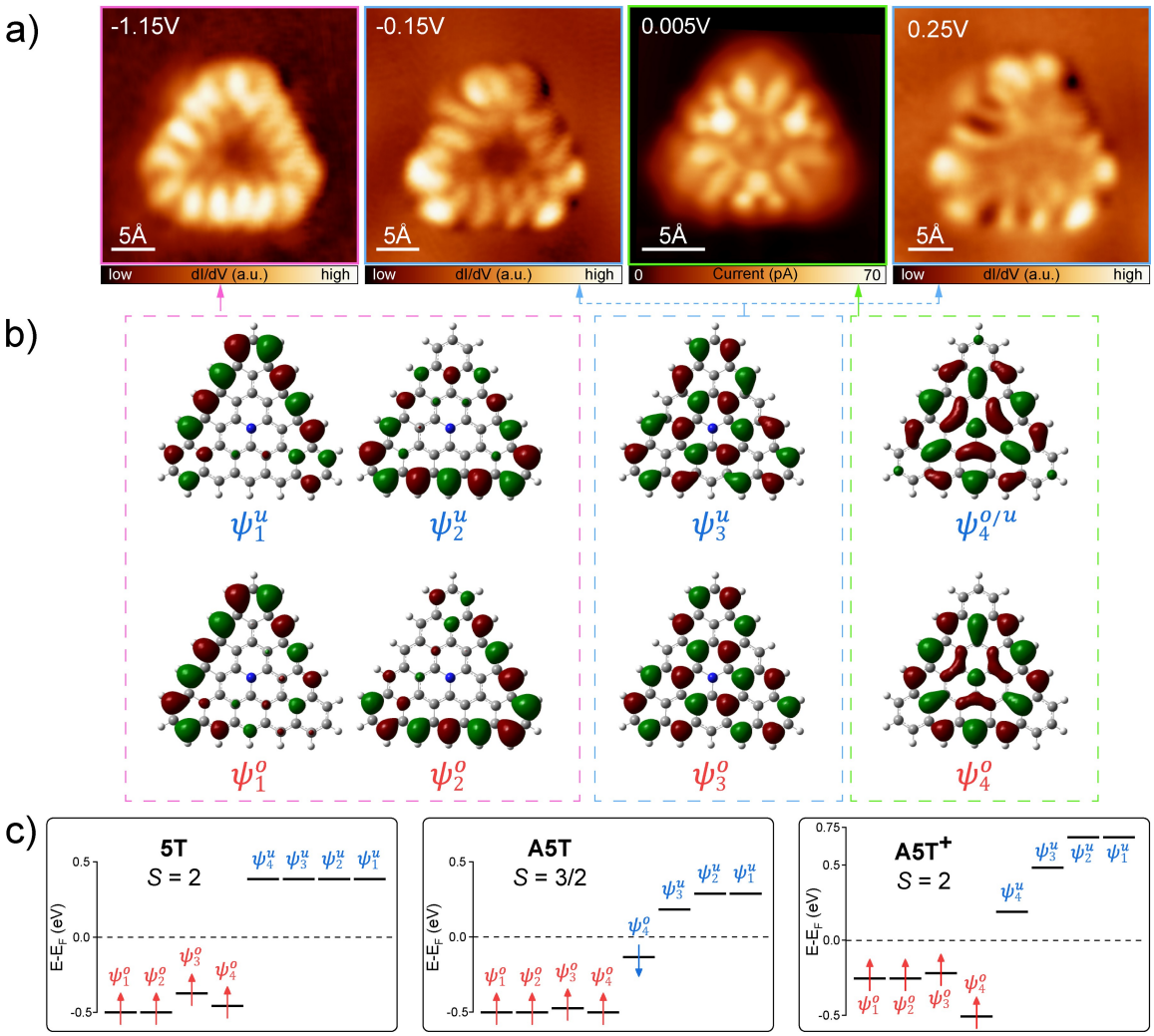

Figure 3. **a)** *dI/dV* maps at different bias acquired at constant current ($I = 500$ pA) of A5T. The map at 0.005 V represents the orbital that contributes the most to the Kondo resonance. For this case, we measured the current instead of dI/dV and used a CO-functionalized tip at larger junction resistances than in BR-STM images. The whole series of *dI/dV* maps is shown in Figure S7. A small asymmetry at the left edge is probably caused by a CO molecule adsorbed at this position. **b)** Molecular orbital isosurfaces of the A5T and the A5T$^+$ of the SOMO and SUMO obtained from spin-polarized DFT. **c)** Energy levels diagram obtained from spin-polarized DFT calculations close to Fermi energy for the case of 5T, A5T, and A5T$^+$.

localization at the zigzag edges of the flakes. In fact, these maps resemble a resonant structure like **A5T-2** in Figure 4a, with radical states delocalized within the middle zigzag edges, rather than the **A5T-1** structure, where radicals lie at the triangulene vertices. Here, we theoretically analyze the (anti)aromaticity of the A5T molecule and show that such an electron delocalization pattern is a fingerprint for the spin state of the flake on the surface.

In Figure 4a we plot the anisotropy of the induced current density (ACID)[54] and the nucleus-independent chemical shift[55] (NICS indices in ppm included in the ACID maps of Figure 4) computed for the A5T molecule in the gas phase. The A5T molecule has a peripheral triangular rim formed by 30 C-atoms, which would fulfill the $4n+2$ Hückel rule for aromaticity if each atom contributed with a π-electron. However, the corresponding ACID plot for a neutral A5T finds a very small ring current around this outer 30-carbon circuit, which is a sign of the global non-aromatic nature of the outer rim. This points to the presence of unpaired electrons at the edges or vertices, reducing the Hückel counting rule, as described by both structures **A5T-1** and **A5T-2** in Figure 4a. In fact, NICS indices find that the benzene rings at the periphery present some (local) aromatic character (NICS(1)zz <0 ppm), with larger negative NICS at the middle-edge rings, and to some extent also at the rings at the vertices. This indicates a larger probability of hosting Clar sextets at these sites,[56] as in **A5T-1** structure. However, the ACID plot of neutral A5T also displays an anticlockwise paramagnetic current flow in the inner rim (thicker C–C bonds in Figure 4a), which can be traced to the [12]annulene moiety present in the **A5T-2** structure, expected to exhibit global antiaromaticity. This is confirmed by the large NICS positive values (NICS(1)$zz = 42.4$ ppm) of the three central rings. Based on this electron delocalization and aromaticity

© 2023 The Authors. Angewandte Chemie International Edition published by Wiley-VCH GmbH

15213773, 2023, 41, Downloaded from https://onlinelibrary.wiley.com/doi/10.1002/anie.202307884 by Universidade de Santiago de Compostela, Wiley Online Library on [31/10/2023]. See the Terms and Conditions (https://onlinelibrary.wiley.com/terms-and-conditions) on Wiley Online Library for rules of use; OA articles are governed by the applicable Creative Commons License

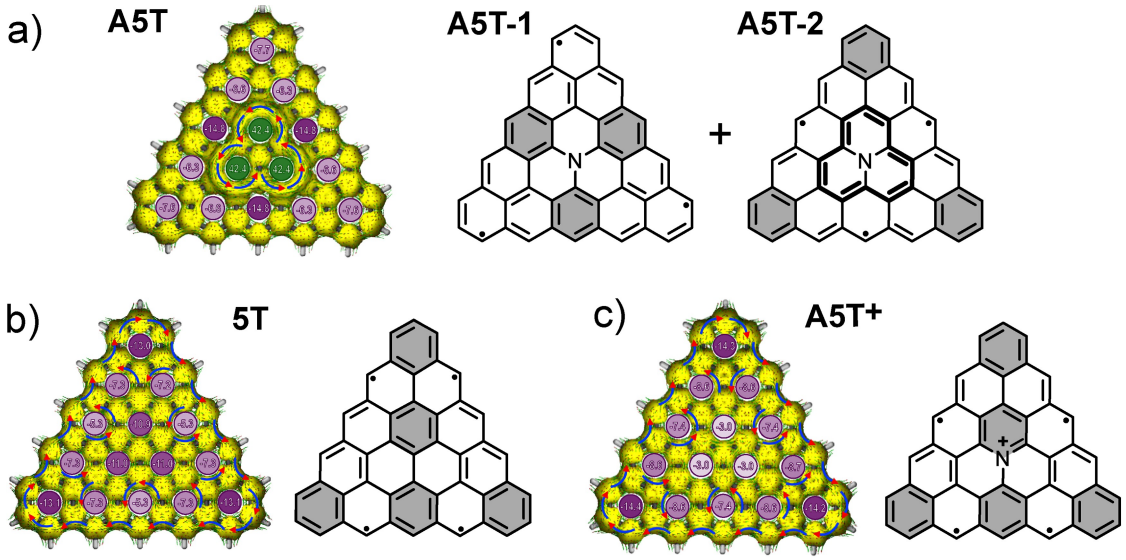

Figure 4. Maps of the computed anisotropy of the induced current density (ACID), for the case of **a)** A5T, **b)** 5T, and **c)** A5T$^+$. Blue arrows are a visualization guide of the direction of the main currents and are unrelated to their magnitude. The numbers inside the benzene rings indicate the nucleus-independent chemical shift ZZ indices 1 Å above the molecular plane (NICS(1)*zz*)1. We also include selected resonance forms for every case. In A5T-2 the thick C–C bonds correspond to the [12]annulene moiety.

indices we conclude that the neutral A5T molecule lies in a superposition of both, the non-aromatic **A5T-1** and the antiaromatic **A5T-2** resonance structures.

The antiaromatic character of the inner rim of A5T contrasts with their aromatic character in the all-carbon 5T flake (Figure 4b). Our simulations (both DFT and MFH) suggest that the local antiaromaticity over the center is brought by the extra π-electron inserted by the aza group, because it doubly populates the state with larger orbital amplitude around the center (ψ_4) and forces the formation of the [12]annulene inner rim. The aza-moiety thus endows the flake with an intrinsic tendency to donate charge by inserting a hole into the doubly occupied ψ_4 state because this reduces the antiaromaticity of the center, a process that is favored by substrates with high electron affinity, such as Au(111).

The A5T$^+$ cation is built up by a hole extending along the ψ_4 orbital (Figure 3b), which is the Kondo screening channel (as shown in the supplementary Figure S10). In fact, the ψ_4-hole contributes to breaking the conjugation of the [12]annulene circuit. The corresponding ACID plot in Figure 4c shows no paratropic currents and a pattern very similar to the all-carbon 5T flake (Figure 4b) appears. The transition from antiaromatic to non-aromatic character is confirmed by NICS(1)*zz* values computed for A5T$^+$ (Figure 4c). The three inner rings become non-aromatic in the cationic flake, and the vertices host now the most aromatic rings (Clar sextet). Therefore, we conclude that the preferential spin localization observed in the experimental Kondo map of Figure 3a (also hinted from the BR-STM images of Figures 1f and 2b), reproduces the features of the cationic character of the A5T$^+$ cation and, hence, confirms its $S=2$ ground state.

In summary, we have described a route to fabricate a large aza-triangulene flake on a metal substrate and demonstrated that it lies in a high-spin state. The fabrication was realized by combining solution synthesis of rationally designed molecular precursors, and on-surface synthesis by thermally induced dehydrogenation reactions. We demonstrated the magnetic state by detecting a very weak Kondo resonance originating from a molecular state with a hole radical caused by charge donation to the surface. Combining experimental orbital maps, Kondo amplitude maps, DFT and MFH simulations, and calculated ACID plots and NICS indices, we determined that the aza-triangulene flake lies in the cationic $S=2$ state on the Au(111) substrate, thus representing a high-spin nanographene. Our work confirms that aza-triangulenes are prone to act as charge donors, to increase their aromatic character.

Acknowledgements

The authors gratefully acknowledge financial support from MCIN/AEI/10.13039/501100011033 through grants No. PID2019-107338RB, PID2019-109555GB-I00, PCI2019-111933-2 and TED2021-132388B-C42, FIS2017-83780-P, and CEX2020-001038-M, from the ELKARTEK project BRTA QUANTUM (no. KK-2022/00041), from the European Regional Development Fund, from the European Union (EU) H2020 program through the FET Open project SPRING (grant agreement No. 863098) and ERC Synergy Grant MolDAM (951519), Xunta de Galicia (Centro de Investigación de Galicia accreditation 2019–2022, ED431G 2019/03) and Xunta de Galicia-Gain Oportunius Program. F.R.-L. thanks the Spanish Ministerio de Educación y Formación Profesional through the PhD scholarship No.

© 2023 The Authors. Angewandte Chemie International Edition published by Wiley-VCH GmbH

15213773, 2023, 41, Downloaded from https://onlinelibrary.wiley.com/doi/10.1002/anie.202307884 by Universidade de Santiago de Compostela, Wiley Online Library on [31/10/2023]. See the Terms and Conditions (https://onlinelibrary.wiley.com/terms-and-conditions) on Wiley Online Library for rules of use; OA articles are governed by the applicable Creative Commons License

FPU20/03305. F.S. acknowledges funding by the Spanish Ministerio de Ciencia e Innovación through Ramón y Cajal Fellowship RYC2021-034304-I. M.E.S.-S. acknowledges the funding by the UK Research and Innovation under the UK government's Horizon Europe funding guarantee (grant number EP/X020908/1). We thank Thomas Frederiksen, Sofía Sanz, and Ricardo Ortiz for fruitful discussions.

Conflict of Interest

The authors declare no conflict of interest.

Data Availability Statement

The data that support the findings of this study are available from the corresponding author upon reasonable request.

Keywords: Bond-Resolved STM · Magnetic Properties · Surface Chemistry · Triangulene · on-Surface Synthesis

[1] W. L. Wang, O. V. Yazyev, S. Meng, E. Kaxiras, *Phys. Rev. Lett.* **2009**, *102*, 157201.
[2] J. Su, M. Telychko, S. Song, J. Lu, *Angew. Chem. Int. Ed.* **2020**, *59*, 7658–7668.
[3] D. G. de Oteyza, T. Frederiksen, *J. Phys. Condens. Matter* **2022**, *34*, 443001.
[4] W. Zeng, J. Wu, *Chem* **2021**, *7*, 358–386.
[5] J. Liu, X. Feng, *Angew. Chem. Int. Ed.* **2020**, *59*, 23386–23401.
[6] A. A. Ovchinnikov, *Theor. Chim. Acta* **1978**, *47*, 297–304.
[7] W. Han, R. K. Kawakami, M. Gmitra, J. Fabian, *Nat. Nanotechnol.* **2014**, *9*, 794–807.
[8] Z. Bullard, E. C. Girão, J. R. Owens, W. A. Shelton, V. Meunier, *Sci. Rep.* **2015**, *5*, 7634.
[9] H. Jin, J. Li, T. Wang, Y. Yu, *Carbon* **2018**, *137*, 1–5.
[10] S. Sanz, N. Papior, G. Giedke, D. Sánchez-Portal, M. Brandbyge, T. Frederiksen, *Phys. Rev. Lett.* **2022**, *129*, 037701.
[11] L. Valenta, M. Juríček, *Chem. Commun.* **2022**, *58*, 10896–10906.
[12] H. Wei, X. Hou, T. Xu, Y. Zou, G. Li, S. Wu, Y. Geng, J. Wu, *Angew. Chem. Int. Ed.* **2022**, *61*, e202210386.
[13] Y. Morita, S. Suzuki, K. Sato, T. Takui, *Nat. Chem.* **2011**, *3*, 197–204.
[14] J. Cai, P. Ruffieux, R. Jaafar, M. Bieri, T. Braun, S. Blankenburg, M. Muoth, A. P. Seitsonen, M. Saleh, X. Feng, K. Müllen, R. Fasel, *Nature* **2010**, *466*, 470–473.
[15] S. Clair, D. G. de Oteyza, *Chem. Rev.* **2019**, *119*, 4717–4776.
[16] N. Pavliček, A. Mistry, Z. Majzik, N. Moll, G. Meyer, D. J. Fox, L. Gross, *Nat. Nanotechnol.* **2017**, *12*, 308–311.
[17] S. Mishra, D. Beyer, K. Eimre, J. Liu, R. Berger, O. Gröning, C. A. Pignedoli, K. Müllen, R. Fasel, X. Feng, P. Ruffieux, *J. Am. Chem. Soc.* **2019**, *141*, 10621–10625.
[18] J. Su, M. Telychko, P. Hu, G. Macam, P. Mutombo, H. Zhang, Y. Bao, F. Cheng, Z.-Q. Huang, Z. Qiu, S. J. R. Tan, H. Lin, P. Jelínek, F.-C. Chuang, J. Wu, J. Lu, *Sci. Adv.* **2019**, *5*, eaav7717.
[19] S. Mishra, K. Xu, K. Eimre, H. Komber, J. Ma, C. A. Pignedoli, R. Fasel, X. Feng, P. Ruffieux, *Nanoscale* **2021**, *13*, 1624–1628.
[20] E. Turco, A. Bernhardt, N. Krane, L. Valenta, R. Fasel, M. Juríček, P. Ruffieux, *JACS Au* **2023**, *3*, 1358–1364.
[21] S. Mishra, D. Beyer, K. Eimre, S. Kezilebieke, R. Berger, O. Gröning, C. A. Pignedoli, K. Müllen, P. Liljeroth, P. Ruffieux, X. Feng, R. Fasel, *Nat. Nanotechnol.* **2020**, *15*, 22–28.
[22] J. Li, S. Sanz, J. Castro-Esteban, M. Vilas-Varela, N. Friedrich, T. Frederiksen, D. Peña, J. I. Pascual, *Phys. Rev. Lett.* **2020**, *124*, 177201.
[23] S. Mishra, D. Beyer, K. Eimre, R. Ortiz, J. Fernández-Rossier, R. Berger, O. Gröning, C. A. Pignedoli, R. Fasel, X. Feng, P. Ruffieux, *Angew. Chem. Int. Ed.* **2020**, *59*, 12041–12047.
[24] S. Mishra, G. Catarina, F. Wu, R. Ortiz, D. Jacob, K. Eimre, J. Ma, C. A. Pignedoli, X. Feng, P. Ruffieux, J. Fernández-Rossier, R. Fasel, *Nature* **2021**, *598*, 287–292.
[25] J. Hieulle, S. Castro, N. Friedrich, A. Vegliante, F. R. Lara, S. Sanz, D. Rey, M. Corso, T. Frederiksen, J. I. Pascual, D. Peña, *Angew. Chem. Int. Ed.* **2021**, *60*, 25224–25229.
[26] J. Su, W. Fan, P. Mutombo, X. Peng, S. Song, M. Ondráček, P. Golub, J. Brabec, L. Veis, M. Telychko, P. Jelínek, J. Wu, J. Lu, *Nano Lett.* **2021**, *21*, 861–867.
[27] S. Cheng, Z. Xue, C. Li, Y. Liu, L. Xiang, Y. Ke, K. Yan, S. Wang, P. Yu, *Nat. Commun.* **2022**, *13*, 1705.
[28] E. Carbonell-Sanromà, J. Hieulle, M. Vilas-Varela, P. Brandimarte, M. Iraola, A. Barragán, J. Li, M. Abadia, M. Corso, D. Sánchez-Portal, D. Peña, J. I. Pascual, *ACS Nano* **2017**, *11*, 7355–7361.
[29] X.-Y. Wang, X. Yao, A. Narita, K. Müllen, *Acc. Chem. Res.* **2019**, *52*, 2491–2505.
[30] N. Friedrich, P. Brandimarte, J. Li, S. Saito, S. Yam-aguchi, I. Pozo, D. Peña, T. Frederiksen, A. Garcia-Lekue, D. Sánchez-Portal, J. I. Pascual, *Phys. Rev. Lett.* **2020**, *125*, 146801.
[31] J. Li, P. Brandimarte, M. Vilas-Varela, N. Merino-Díez, C. Moreno, A. Mugarza, J. S. Mollejo, D. Sánchez-Portal, D. Garcia de Oteyza, M. Corso, A. Garcia-Lekue, D. Peña, J. I. Pascual, *ACS Nano* **2020**, *14*, 1895–1901.
[32] N. Friedrich, R. E. Menchón, I. Pozo, J. Hieulle, A. Vegliante, J. Li, D. Sánchez-Portal, D. Peña, A. Garcia-Lekue, J. I. Pascual, *ACS Nano* **2022**, *16*, 14819–14826.
[33] E. C. H. Wen, P. H. Jacobse, J. Jiang, Z. Wang, R. D. McCurdy, S. G. Louie, M. F. Crommie, F. R. Fischer, *J. Am. Chem. Soc.* **2022**, *144*, 13696–13703.
[34] R. E. Blackwell, F. Zhao, E. Brooks, J. Zhu, I. Piskun, S. Wang, A. Delgado, Y.-L. Lee, S. G. Louie, F. R. Fischer, *Nature* **2021**, *600*, 647–652.
[35] T. Wang, A. Berdonces-Layunta, N. Friedrich, M. Vilas-Varela, J. P. Calupitan, J. I. Pascual, D. Peña, D. Casanova, M. Corso, D. G. de Oteyza, *J. Am. Chem. Soc.* **2022**, *144*, 4522–4529.
[36] M. M. Ugeda, I. Brihuega, F. Guinea, J. M. Gómez-Rodríguez, *Phys. Rev. Lett.* **2010**, *104*, 096804.
[37] H. González-Herrero, J. M. Gómez-Rodríguez, P. Mal-let, M. Moaied, J. J. Palacios, C. Salgado, M. M. Ugeda, J.-Y. Veuillen, F. Yndurain, I. Brihuega, *Science* **2016**, *352*, 437–441.
[38] M. E. Sandoval-Salinas, A. Carreras, D. Casanova, *Phys. Chem. Chem. Phys.* **2019**, *21*, 9069–9076.
[39] C. Chen, J. Lu, Y. Lv, Y. Yan, Q. Sun, A. Narita, K. Müllen, X.-Y. Wang, *Angew. Chem. Int. Ed.* **2022**, *61*, e202212594.
[40] J. Brede, N. Merino-Díez, A. Berdonces, S. Sanz, A. Domínguez-Celorrio, J. Lobo-Checa, M. Vilas-Varela, D. Peña, T. Frederiksen, J. I. Pascual, D. G. de Oteyza, D. Serrate, *arXiv* **2023**, https://doi.org/10.48550/arXiv.2301.11370.
[41] J. Kondo, *Prog. Theor. Phys.* **1964**, *32*, 37–49.
[42] M. Ternes, A. J. Heinrich, W.-D. Schneider, *J. Phys. Condens. Matter* **2009**, *21*, 053001.
[43] J. Li, S. Sanz, M. Corso, D. J. Choi, D. Peña, T. Frederiksen, J. I. Pascual, *Nat. Commun.* **2019**, *10*, 200.
[44] J. J. Parks, A. R. Champagne, T. A. Costi, W. W. Shum, A. N. Pasupathy, E. Neuscamman, S. Flores-Torres, P. S. Cornaglia,

© 2023 The Authors. Angewandte Chemie International Edition published by Wiley-VCH GmbH

15213773, 2023, 41, Downloaded from https://onlinelibrary.wiley.com/doi/10.1002/anie.202307884 by Universidade de Santiago de Compostela, Wiley Online Library on [31/10/2023]. See the Terms and Conditions (https://onlinelibrary.wiley.com/terms-and-conditions) on Wiley Online Library for rules of use; OA articles are governed by the applicable Creative Commons License

A. A. Aligia, C. A. Balseiro, G. K.-L. Chan, H. D. Abruña, D. C. Ralph, *Science* **2010**, *328*, 1370–1373.
[45] W. L. Wang, S. Meng, E. Kaxiras, *Nano Lett.* **2008**, *8*, 241–245.
[46] H. O. Frota, *Phys. Rev. B* **1992**, *45*, 1096–1099.
[47] M. Gruber, A. Weismann, R. Berndt, *J. Phys. Condens. Matter* **2018**, *30*, 424001.
[48] M. Ternes, *New J. Phys.* **2015**, *17*, 063016.
[49] L. Gross, F. Mohn, N. Moll, P. Liljeroth, G. Meyer, *Science* **2009**, *325*, 1110–1114.
[50] G. Kichin, C. Weiss, C. Wagner, F. S. Tautz, R. Temirov, *J. Am. Chem. Soc.* **2011**, *133*, 16847–16851.
[51] E. Clar in *Mobile Source Emissions Including Policyclic Organic Species* (Eds.: D. Rondia, M. Cooke, R. K. Haroz), Springer Netherlands, Dordrecht, **1983**, pp. 49–58.
[52] M. Solà, *Front. Chem.* **2013**, *1*, 2296–2646.
[53] B. de la Torre, M. Švec, G. Foti, O. Krejčí, P. Hapala, A. Garcia-Lekue, T. Frederiksen, R. Zbořil, A. Arnau, H. Vázquez, P. Jelínek, *Phys. Rev. Lett.* **2017**, *119*, 166001.
[54] D. Geuenich, K. Hess, F. Köhler, R. Herges, *Chem. Rev.* **2005**, *105*, 3758–3772.
[55] P. R. von Schleyer, H. Jiao, *Pure Appl. Chem.* **1996**, *68*, 209–218.
[56] G. Portella, J. Poater, M. Solà, *J. Phys. Org. Chem.* **2005**, *18*, 785–791.
[57] I. Horcas, et al., *Rev. Sci. Instrum.* **2007**, *78*, 013708.
[58] J. P. Perdew, K. Burke, M. Ernzerhof, *Phys. Rev. Lett.* **1996**, *77*, 3865.
[59] J. M. Soler, E. Artacho, J. D. Gale, A. García, J. Junquera, P. Ordejón, D. Sánchez-Portal, *J. Phys. Condens. Matter* **2002**, *14*, 2745.
[60] M. J. Frisch et al. https://gaussian.com/citation/ Gaussian09 Revision D.01. **2013**.
[61] S. Sanz, N. Papior, T. Frederiksen, https://doi.org/10.5281/zenodo.4748765 Zenodo **2022**, v0.2.0.

Manuscript received: June 5, 2023
Accepted manuscript online: August 21, 2023
Version of record online: September 6, 2023

© 2023 The Authors. Angewandte Chemie International Edition published by Wiley-VCH GmbH

15213773, 2023, 41, Downloaded from https://onlinelibrary.wiley.com/doi/10.1002/anie.202307884 by Universidade de Santiago de Compostela, Wiley Online Library on [31/10/2023]. See the Terms and Conditions (https://onlinelibrary.wiley.com/terms-and-conditions) on Wiley Online Library for rules of use; OA articles are governed by the applicable Creative Commons License